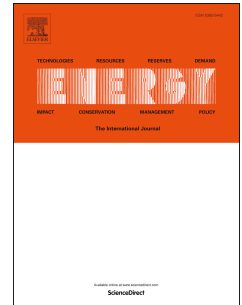


Journal Pre-proof

Enhancing solar chimney performance in urban tunnels: Investigating the impact factors through experimental and theoretical model analysis

Youbo Huang, Xi Liu, Long Shi, Bingyan Dong, Hua Zhong



PII: S0360-5442(23)01723-1

DOI: <https://doi.org/10.1016/j.energy.2023.128329>

Reference: EGY 128329

To appear in: *Energy*

Received Date: 11 January 2023

Revised Date: 14 June 2023

Accepted Date: 2 July 2023

Please cite this article as: Huang Y, Liu X, Shi L, Dong B, Zhong H, Enhancing solar chimney performance in urban tunnels: Investigating the impact factors through experimental and theoretical model analysis, *Energy* (2023), doi: <https://doi.org/10.1016/j.energy.2023.128329>.

This is a PDF file of an article that has undergone enhancements after acceptance, such as the addition of a cover page and metadata, and formatting for readability, but it is not yet the definitive version of record. This version will undergo additional copyediting, typesetting and review before it is published in its final form, but we are providing this version to give early visibility of the article. Please note that, during the production process, errors may be discovered which could affect the content, and all legal disclaimers that apply to the journal pertain.

© 2023 Published by Elsevier Ltd.

Youbo Huang: Formal analysis, Project administration, supervision, writing the original draft.

Xi Liu: Data curation, writing, review & editing.

Long Shi: Conceptualization, Writing - review & editing, Methodology, Supervision, Resources.

Bingyan Dong: Data curation, writing, review & editing.

Hua Zhong: Methodology, Writing - review & editing.

Enhancing solar chimney performance in urban tunnels: Investigating the impact factors through experimental and theoretical model analysis

Youbao Huang^a, Xi Liu^a, Long Shi^{b,c*}, Bingyan Dong^a, Hua Zhong^{d**}

^a College of Safety Engineering, Chongqing University of Science and Technology, Chongqing 401331, China

^b State Key Laboratory of Fire Science, University of Science and Technology of China, Hefei, Anhui 230026, China

^c School of Architecture and Civil Engineering, Chengdu University, Chengdu, 610106, Sichuan, China

^d School of Architecture, Design and Built Environment, Nottingham Trent University, Nottingham NG1 4FQ, United Kingdom

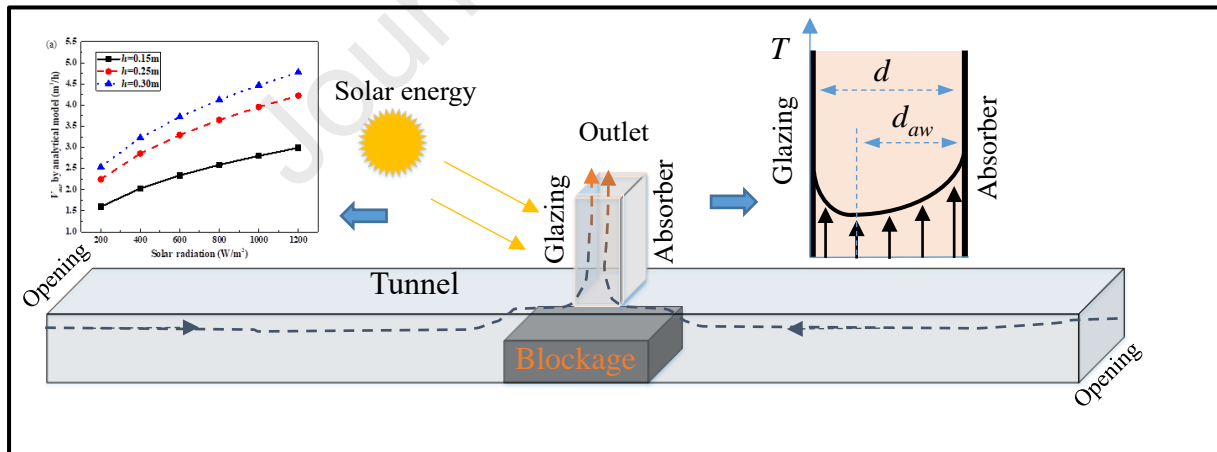
*Corresponding author: shilong@ustc.edu.cn (L. Shi) hua.zhong@ntu.ac.uk (H. Zhong)

Abstract

Efficient and sustainable ventilation in urban tunnels is crucial for combating air pollution and safeguarding human health. This study investigates the design factors impacting solar chimney performance in urban tunnels to optimize ventilation efficiency. Experimental trials analyzed the effects of blockage ratio, chimney height, and solar radiation on temperature distribution and ventilation rate. The results demonstrate that increased chimney height and solar radiation positively influence airflow velocity at the chimney outlet, enhancing ventilation. The temperature rise near absorber is higher than that closed to glazing wall. Temperature distribution within the chimney follows a distinctive horizontal two-pieewise semi-parabolic decay pattern, enabling accurate prediction of temperature profiles along the cavity depth. Novel analytical models predict temperature distribution, airflow velocity, and ventilation rate within the solar chimney system, aiding precise design and optimization. Remarkably, the blockage ratio has limited impact on ventilation rate, allowing for disregarding vehicle blockage effects in solar chimney design for urban tunnels. Matching chimney width to tunnel width and ensuring a relatively high chimney height are emphasized for optimal functionality. The study holds substantial implications for ventilation system design in urban environments, promoting healthier and more sustainable cities.

Keywords: solar chimney, urban tunnel, natural ventilation, renewable energy, the theoretical model

Graphical Abstract



Nomenclature

A	Area (m ²)	u_c	Airflow velocity inside the channel (m/s)
$A_{blo.}$	Area in blockage region (m ²)	u_{in}	Velocity at the inlet (m/s)
A_c	Chimney cavity area (m ²)	u_{max}	Maximum velocity at the centreline of the channel (m/s)
A_{in}	Cavity inlet area (m ²)	u_{out}	Velocity at the outlet (m/s)
A_t	Cross-section area of the tunnel (m ²)	u_s	Velocity outside the boundary layer (m/s)
C_d	Discharge coefficient	u_t	Airflow velocity in the tunnel (m/s)
c_p	Specific heat capacity (J/(kg·K))	ν	Kinetic viscosity of air (m ² /s)
D_c	Hydraulic diameter of the cavity (m)	V	Volume flow rate (m ³ /s)
D_t	Hydraulic diameter of tunnel (m)	V_{out}	Volume flow rate at the outlet (m ³ /s)
d	Chimney cavity depth (m)	w	Chimney cavity width (m)
d_{aw}	Horizontal distance from the absorber position's lowest temperature (m)	<i>Greek symbols</i>	
E	Power of heating source (kW)	β	Blockage ratio
E_{aw}	Energy absorbed by the absorption wall (kW)	δ	Boundary layer thickness (m)
E_{gw}	Energy absorbed by the glazing wall (kW)	ε	Absorptivity of glazing wall
Gr	Grashof number	ζ	Local resistance coefficient
h	Chimney cavity height (m)	ζ_{blo}	Resistance coefficient as blockage
L_t	Tunnel length (m)	ζ_{en}	Resistance coefficient at the tunnel entrance
Pr	Prandtl number	ζ_{in}	Resistance coefficient at the inlet
ΔP_ζ	Local resistance (Pa)	ζ_{out}	Resistance coefficient at the discharge outlet
ΔP_λ	Friction resistance (Pa)	κ	Coefficient.
q	Heat flux (kW/m ²)	λ	Friction resistance coefficient
R	The radius of the channel (m)	ρ	Density (kg/m ³)
r	Distance from wall (m)	ρ_0	Ambient density (kg/m ³)
T	Temperature (K)	ρ_c	Density in a chimney cavity (kg/m ³)
T_0	Ambient temperature (K)	ρ_{out}	Air density at the outlet (kg/m ³)
$T_{aw, max}$	Temperature closed to absorption wall (K)	τ	Transmissivity of the glazing wall
T_c	Temperature inside the chimney cavity (K)	<i>Subscripts and Superscripts</i>	
$T_{gw, max}$	Temperature closed to glaze wall (K)	aw	Absorption wall
T_{max}	Maximum temperature (K)	$blo.$	Blockage
T_{out}	Temperature at the outlet (K)	c	Chimney cavity
ΔT	Temperature difference (K)	en	Tunnel entrance
u	Airflow velocity (m/s)	gw	Glazing wall
$u_{blo.}$	Airflow velocity in the blockage region (m/s)	in	Chimney cavity inlet
		max	Maximum value
		out	Chimney cavity outlet

1 Introduction

Urban tunnels, as a topic of traffic development in large and middle-sized cities, have been constructed rapidly to relieve urban centre traffic pressure and save urban land [1]. With the increase in traffic volume in urban tunnels, the poor air quality inside would cause various adverse respiratory and cardiovascular health problems for commuters, drivers, and residents in neighbouring communities [2]. A ventilation system, including a mechanical energy driving system or natural shaft, was used to exhaust the pollution and entrain the fresh air. Mechanical ventilation systems are widely used to exchange polluted air and prevent smoke movement in urban tunnels [3, 4]. Currently, electricity is used to drive the mechanical ventilation system, with the annual electricity costs of the ventilation system taking up over 70% of its operating energy consumption (only 20% for illumination) in the Zhongnanshan Highway Tunnel in China [5]. The energy consumption of mechanical ventilation systems in metros contributes to 55% of the energy used for contraction purposes [6]. This large electricity consumption (68%

produced by fossil fuels) for tunnel ventilation systems costs lots of fossil fuels, raising energy crises and environmental problems due to pollution released during processing [7]. During fire accident conditions in the tunnel, a forced ventilation system needs to be constructed and booted up to overcome the smoke movement [4]. Under this circumstance, the energy consumption would be further aggravated.

The shaft natural ventilation systems with low energy consumption have attracted much attention that always combines with a jet fan system to reduce energy consuming in the tunnel. The horizontal ventilation caused by the jet fan eliminates the polluted emission of the vehicle through the shaft under operation mode, and the shaft venting exhausts the hot smoke under fire conditions. For a 11377 m long tunnel, using a vertical shaft combined with a jet fan can save electricity charges of CNY 308,790 per year [8]. Engineering cases showed that shaft natural ventilation combined with jet fans could reduce tunnel operating costs by 20-35% annually[9]. However, only the natural shaft shows a limited ventilation rate due to a lack of driving kinetic energy. Thus, the jet fans are always combined with the shaft to create sufficient momentum inducing airflow and overcoming smoke movement under fire conditions, resulting in limited energy-saving but construction costs for natural shaft ventilation. A renewable energy ventilation system with optimal ventilation performance is necessary for the tunnel.

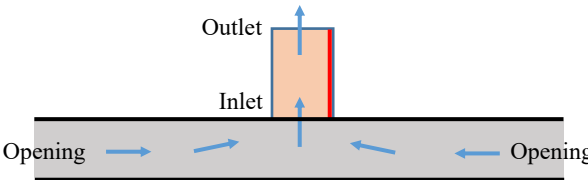
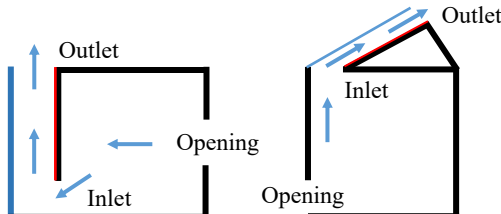
A solar chimney (SC), which consists of a chimney cavity (glazing wall and absorption wall) and airflow opening (inlet and outlet)[10], is frequently integrated into building ventilation [11, 12] and power generation to save energy [13-15]. The solar chimney absorbed solar radiation to heat the internal air inside the cavity. The temperature difference between indoor spacing and a chimney cavity induces a difference in air density. The thermal buoyancy drives the airflow to achieve the purpose of ventilation and air exchange indoor spacing. Applying solar chimneys in building ventilation can help reduce electricity consumption and gas emissions [16]. Miyazaki et al. [17] concluded that solar chimney ventilation systems can reduce fan shaft power requirements by 50% annually in Japan. The Solar natural ventilation adopted in buildings saves almost 10-15% of the annual fan power requirement [18] and enhances the air changes per hour indoors under more convenient operational and climatic conditions [19]. A solar chimney can simultaneously implement room heat and ventilation, such as a Trompe wall. The energy saving by reduced electricity consumption for building heating and ventilation is obvious as reducing greenhouse gas emissions [20].

The extensively used solar chimney in buildings has achieved good energy savings, while its application in tunnels (underground spacing) has rarely been reported and studied. Following the same principle, the solar chimney is viable for its applications in tunnels and has been investigated numerically by Cheng *et al.* [10]. Most urban tunnels are just a couple of meters below the ground, making it feasible to adopt solar chimneys, such as urban traffic link tunnels [21, 22] and Metro Shallow Buried Interval Tunnels. Otherwise, the vertical shaft has always been applied in the tunnel to improve ventilation performance and illumination [23]. The solar energy integrated into the vertical shaft could accelerate the airflow velocity in the tunnel, generating the stack effect. Because solar radiation heats the internal air, the thermal gradient results in a significant density difference. Thus, using the solar chimney to replace the conventional vertical shaft has energy-saving and functional stability merits. However, the corresponding research barely exists, and experimental investigation is rarely reported. When a solar chimney is applied in the tunnel, the related influence of solar chimney configuration on ventilation performance may be quite different from that of buildings because of different structure and airflow characteristics (as shown in Table 1). The related in-depth theoretical analysis model is critical and significant to quantify this effect and expand the application of solar chimneys in a practical tunnel. Therefore, the experiment is critically needed to investigate the ventilation performance of solar chimneys in the tunnel and confirm its application. Developing a theoretical model is crucial to quantify the influences of realistic designing factors on ventilation performance and guide the practical applications.

Although the theoretical model for solar chimneys has been studied over the past decades, these models are mainly for building ventilation [16, 18, 24]. In the previous analytical model, the temperature distribution inside the cavity was assumed to be uniform [25]. The vertical linear temperature distribution combined with horizontal parabolic temperature has also been conducted to establish a theoretical model for a tunnel solar chimney [10]. Sengupta found that the inside temperature adjusting to the absorption wall is higher than near the glazing wall [26]. He et al. [27] and Gong et al. [28] also found that the temperature near the external glazing wall surface is lower than that adjusted to the back-absorbed wall [29]. However, a quantitative assessment of the effect of asymmetric temperature distribution on solar chimney performance is lacking. This gives rise to the difficulty of applying solar chimneys in tunnels and design. The diversity of real-life applications raises a

great need for developing simplified mathematical methods capable of hand-calculating the ventilation rates for the case of solar chimneys adopted in tunnels.

Table 1 Difference in solar chimney integrated into building and tunnel

	Solar chimney in the tunnel	Typical solar chimney in a building
Schematic		
Structure type	Long-narrow space	Chamber space
Airflow opening	Two entrances	One opening
Location	Underground	Ground
Chimney type	Top vertical	Side vertical / Roof inclined
Airflow feature	Confluence flows into the cavity	Single flow into the cavity

This study conducted experiments to investigate the ventilation performance of a solar chimney in an urban tunnel. This research aims to understand the ventilation potential of a thermal-driven solar chimney in a tunnel and to establish a global analytical model for estimating the ventilation rate of a solar chimney installed in a tunnel. The influences of solar radiation, blockage ratio of the vehicle, and solar chimney height on the ventilation performance of the solar chimney at the top of a tunnel were determined. An analytical model for the temperature distribution and airflow velocity in the cavity depth direction is developed by considering the asymmetric parabolic temperature profile inside the solar chimney cavity. Ultimately, a simple-to-use analytical model is established to predict the ventilation rate throughout a solar chimney in realistic scenarios.

2 Experimental methodologies

2.1 Solar chimney in the tunnel

A series of experiments were conducted for a roof solar chimney in the tunnel, as shown in Fig.1. The model tunnel was 10 m in length, 0.5 m in width and 0.25 m in height. The front sidewall of the tunnel was constructed using transparent fireproof glass (conductivity $1.2 \text{ W} / (\text{m} \cdot \text{K})$) with a thickness of 5 mm to provide visual observation inside the tunnel. The other walls of the model tunnel were made of 1.5 mm stainless steel plate with thermal conductivity of $12.1 \text{ W}/(\text{mK})$. A solar chimney was installed at the top of the tunnel. The width of the chimney cavity (w) was 150 mm, and the cavity depth (d) was 100 mm (all internal sizes). Three cavity heights (h) of 150 mm, 250 mm, and 300 mm were conducted. Two sidewalls of the solar chimney cavity were constructed using 10-mm-thick extruded polystyrene (XPS) and a 3-mm-thick aluminium plate wrapped around the XPS from the periphery. The absorption wall was constructed using a 5-mm thick black fireproof. A 5-mm thick aerogel composite board was attached to the absorption wall (fireproof board) for insulation purposes [30]. The aerogel composite board (ACB) was wrapped using a 3 mm thick aluminium plate from the periphery, as shown in Fig.1 (b). The front wall of the solar chimney was made using 3 mm thick transparent glazing with a thermal conductivity of $0.76 \text{ W} / (\text{m} \cdot \text{K})$. Artificial lights were used to simulate the sunshine [30]. The artificial lights included eight rows of iodine-tungsten lamps with a 3×36 array and 864 lamp beads. These lamps are used to simulate solar radiation, which can provide uniform radiation heat on the glazing wall within a range of $0\text{-}2000 \text{ W}/\text{m}^2$. The radiation intensity is varied by controlling the distance between the lamps and the solar chimney. A light intensity radiometer (SM206, with an accuracy of $0.1 \text{ W}/\text{m}^2$, ranging from 0 to $2000 \text{ W}/\text{m}^2$) was employed to measure the radiation intensity over the glazing surface. The artificial light penetrates the transparent glazing wall and heats the inside air. Three solar radiation intensities of $400 \text{ W}/\text{m}^2$, $600 \text{ W}/\text{m}^2$ and $800 \text{ W}/\text{m}^2$ were measured.

Three different blockage ratios inside the tunnel (the ratio of blockage cross-section area to tunnel cross-section area) were conducted to investigate the effect of the vehicle or train on the airflow performance induced by the solar chimney, which was 0, 0.12 and 0.24. To provide a stable test environment, the experiments were conducted in a large indoor laboratory where the wind velocity was zero.

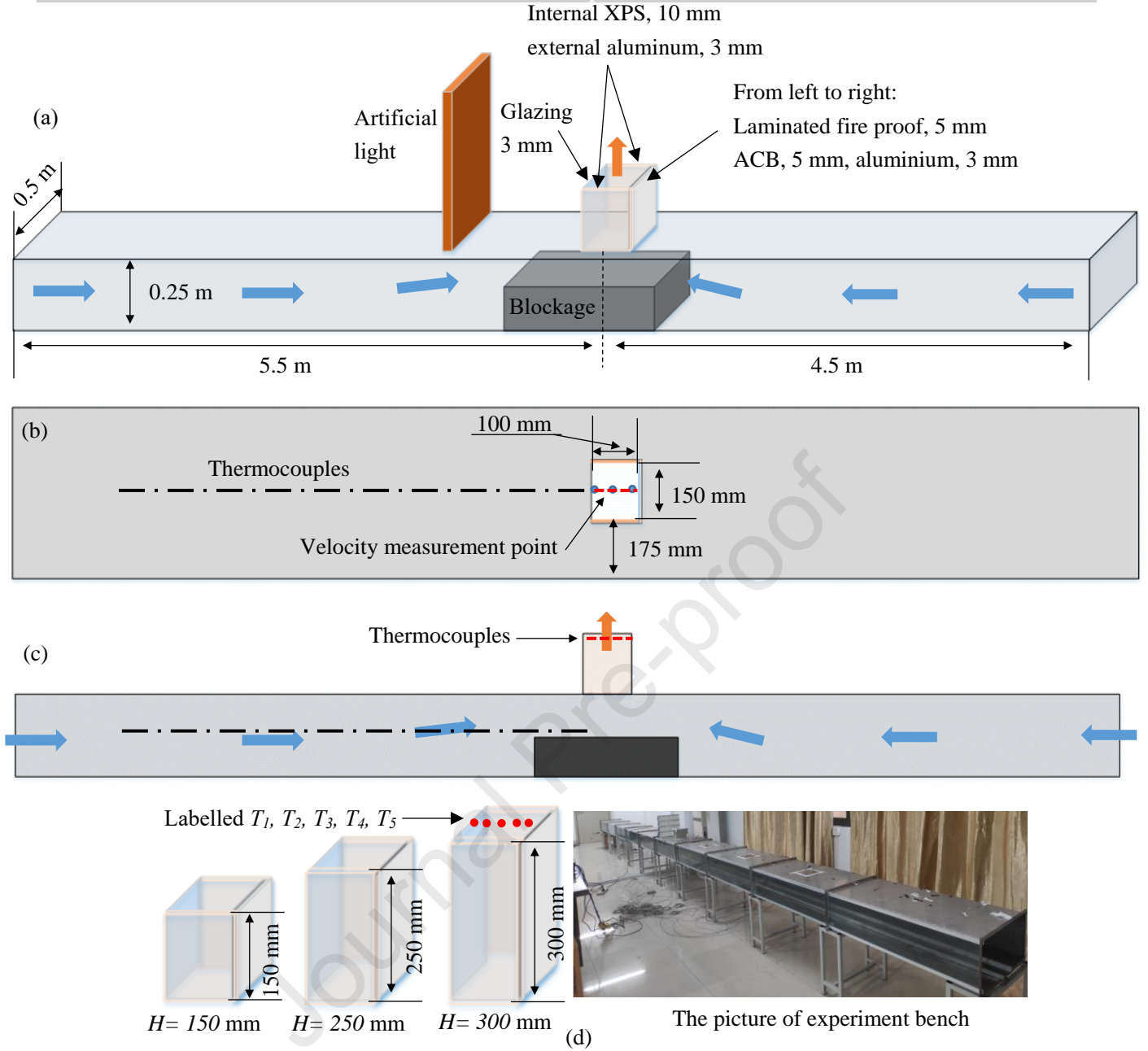


Fig. 1 Schematic of the solar chimney in a tunnel: (a) 3D model of the experimental platform, (b) top view, (c) front view, (d) from left to right: three cavities with different height, picture of experiment bench.

2.2 Measurement system

A hot-wire anemometer (KANOMAX model KA12) with four channels (1CH – 4CH) was used to detect the outlet velocity. Three measurement positions along the chimney cavity depth were installed at an interval of 45 mm away from the glazing wall: 5, 50 and 95 mm. The accuracy of the measured velocity is 0.01m/s.

One cluster includes five thermocouples arranged in the chimney cavity depth direction at the outlet. The thermocouples from left to right are labelled as T_1, T_2, T_3, T_4 and T_5 away from the left glazing wall 5 mm, 20 mm, 50 mm, 80 mm and 95 mm, respectively. That means T_1 closes to the glazing wall's internal surface, T_5 closes to the internal surface of the absorber wall, and T_3 is in the centre position. The array inside the solar chimney cavity is shown in red in Fig. 1 (d). Eleven thermocouples were used to measure the longitudinal temperature at the tunnel centreline, which were placed on the left side with an interval of 0.4 m, shown as a dotted line in Fig. 1. All the thermocouples in this experiment are K-type with 1 mm diameter. The range of measurement was from -100°C to 1500°C with an accuracy of 1.0°C and $\pm 0.05\%$. A data acquisition system (Keysight DAQ970A) was used to collect the measured signal and transform the information into a PC.

2.3 Experimental scenarios

Table 1 lists 27 experimental cases. Three chimney cavity heights of 150, 25, and 300mm were conducted. The blockage ratio ranged from 0 to 0.24, and the solar radiation varied from 400W/m^2 to 800W/m^2 with an interval of 200W/m^2 . The artificial light was turned on to preheat the glazing before the test, ensuring uniform solar radiation intensity. The measurement duration was 1.5 h. The results of velocity showed that the system reached a quasi-steady state at approximately 3000s, as shown in Fig. 2 (a). Thus, the measured data during the quasi-steady state were used for the following analysis. Each test was repeated three times to address the repeatability of the experiments. The results showed good repeatability of the experimental rig, with details shown in Fig. 2 (b).

Table 1 Summary of test conditions.

No.	Cavity height (mm)	The solar radiation (W/m^2)	Blockage ratio
1-3	150	400	0, 0.12, 0.24
4-6	150	600	
7-9	150	800	
10-12	250	400	
13-15	250	600	
16-18	250	800	
19-21	300	400	
22-24	300	600	
25-27	300	800	

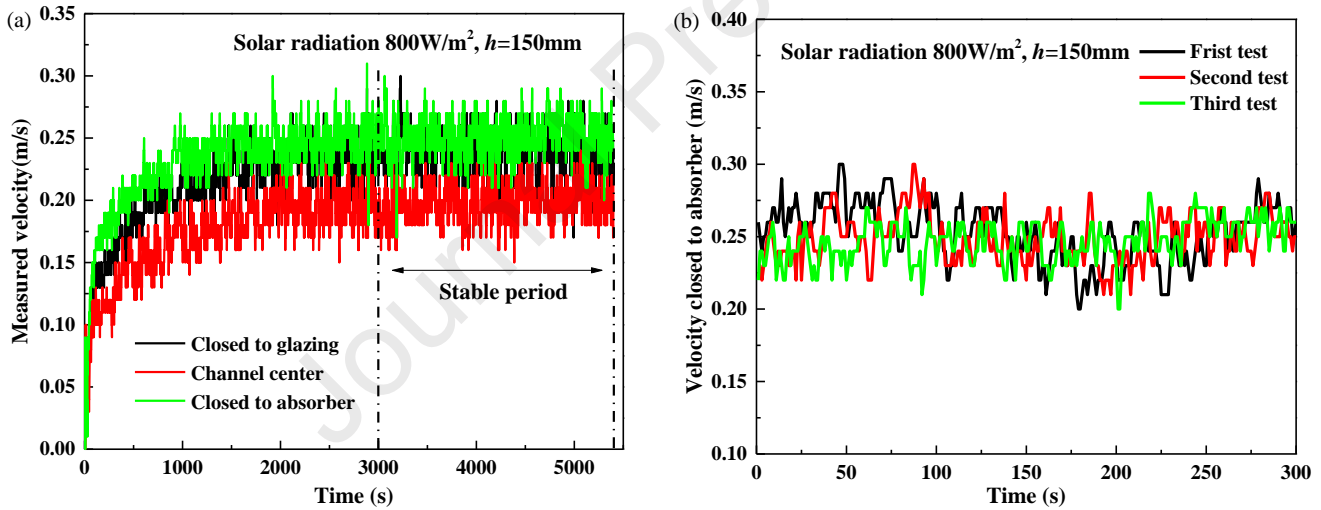


Fig. 2 Measured data during the test process with solar radiation 800W/m^2 , cavity height 150 mm and no blockage: (a) stabilization of the measured velocity, (b) repeatability of velocity closed to the absorbed wall during steady state.

3 Results and discussion

3.1 Without blockage

Solar radiation is an essential factor for the optimization design of solar chimneys as it provides varied thermal intensity. Fig. 3(a) shows the typical outlet temperature distribution along the cavity depth direction, where the cavity height is 150 mm without blockage. The air temperatures at the outlet were non-uniform, like two semi-parabolic attenuate curves from the opposite wall to the centre. The temperature in the depth direction decreased to the minimum value and then increased away from the glazing wall. The temperature near the glazing wall surface increased slightly but was lower than that adjusted to the absorption wall [29, 31]. The air temperature near the absorption wall was the highest. The maximum temperature difference between the glazing and absorption walls can rise to 7°C under solar radiation 800W/m^2 . The solar energy transits the glazing wall and is absorbed by black fireproof. The absorption surface has been heated, resulting in the highest temperature over this side. Due to the convective heat transfer, the temperature decreased from the absorption wall to the cavity centre. In the present

experiments, the temperature over the internal glazing surface was relatively high due to the absorbance of the glazing. Previous researchers also found that the temperature decreased gradually as the distance from the heated back wall increased [27-29]. Fig. 3(b) shows the temperature along the tunnel centreline kept stable. Additionally, solar radiation shows a limited impact on the temperature in the tunnel.

The lowest temperature rise at the outlet was achieved at 3 °C under radiation heat flux 400 W/m². The highest temperature rises adjusted to the absorption wall was 33 °C, 37.4 °C, and 41.7 °C under radiation intensities of 400 W/m², 600 W/m², and 800 W/m², respectively. The average temperature is usually predicted using the heat balance given in Eq.1. Obviously, it is applied only to the uniform temperature profile. Therefore, the average temperature analysed using the heat balance method is unsuitable for predicting the temperature gradient inside this solar chimney cavity.

$$\Delta T = \frac{qh}{du\rho c_p} \quad (1)$$

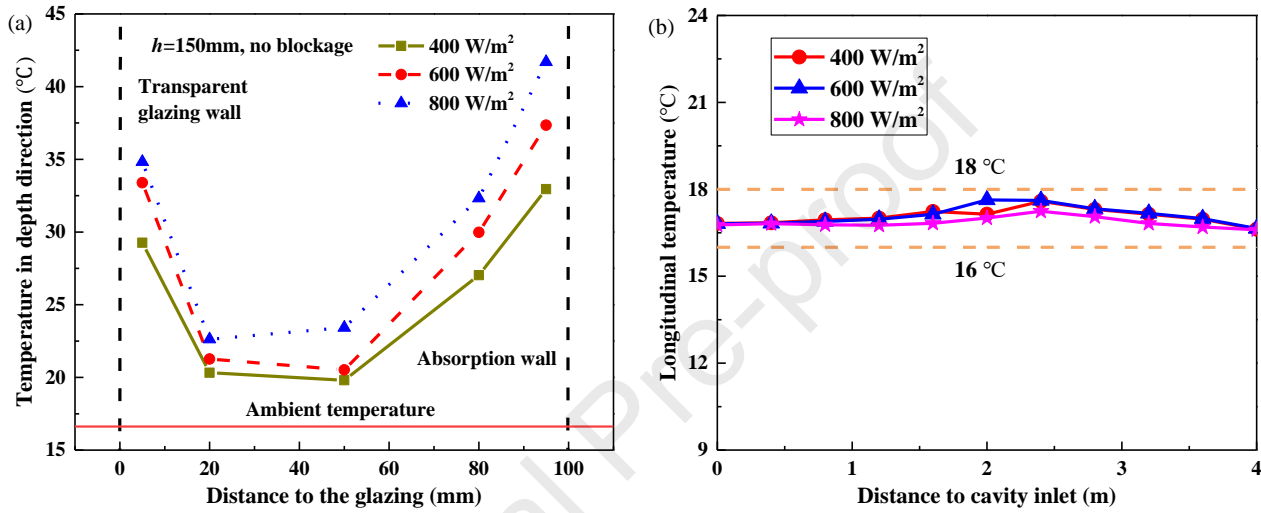


Fig.3 Measured temperature results (a) in the cavity depth direction and (b) along the tunnel centreline.

Figure 4 reveals the velocity through the air outlet without blockage. The velocity adjusted to the glazing and absorption walls both increased with increasing solar radiation [32]. The reason is that the greater solar radiation enhances the temperature gradient between the airflow inside and outside the solar chimney cavity, which produces a stronger stack effect to drive the airflow. The cavity height significantly affected the airflow velocity adjusted to the absorption wall. The higher cavity height means a larger total absorption wall area; thus, more radiation flux is absorbed to heat inflow air. Consequently, the airflow velocity was greater with higher cavity height due to the enhancement of the stack effect [10]. However, the airflow velocity over the glazing wall surface was insensitive to the cavity height when h was larger than 250 mm. Because most solar radiation is absorbed by the back absorption wall, the absorption coefficient of transparent glazing is relatively small, while the heat dissipates quickly from the glazing. Low heat absorption and large heat dissipation result in less thermal storage to improve the surface temperature. Thus, the cavity height has a limited impact on airflow velocity over the glazing wall surface.

For turbulent flow, an approximation model for the cross-section velocity has been developed [27, 33], expressed as Eq. (2). Unfortunately, this model is only applied for round flow with velocity decreasing gradually from the centreline of the pipe to the boundary layer, which has not considered the influence of thermal buoyance. It has been noted that it is unsuitable for the airflow velocity profile inside the solar chimney channel. For thermal boundary layer flow, the cross-section velocity is dependent mainly on the thermal boundary layer thickness. Eq. (3) can be used to calculate the airflow velocity at an axial distance [34]. Based on Eckert's study, Hou *et al.* [29] proposed different power coefficients and constants to predict u_s and δ .

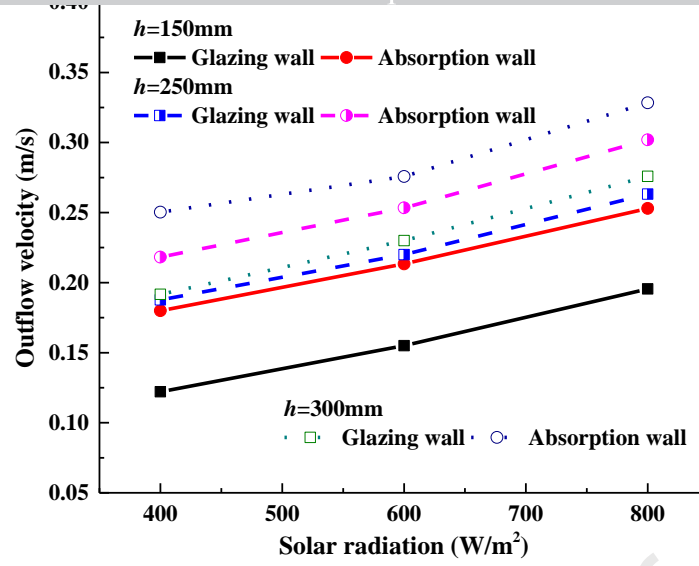


Fig. 4 Airflow velocity at the outlet without blockage.

$$u = u_{\max} \left(1 - \frac{r}{R} \right)^{1/7} \quad (2)$$

$$u = u_s \frac{r^{1/7}}{\delta} \left(1 - \frac{r}{\delta} \right)^4 \quad (3)$$

$$\delta = 0.505 Gr^{-1/14} Pr^{-1/2} \left(1 + 0.445 Pr^{2/3} \right)^{1/14} r \quad (4)$$

$$u_s = 4.35 \frac{\nu}{r} Gr^{5/14} Pr^{-1/16} \left(1 + 0.445 Pr^{2/3} \right)^{-5/14} \quad (5)$$

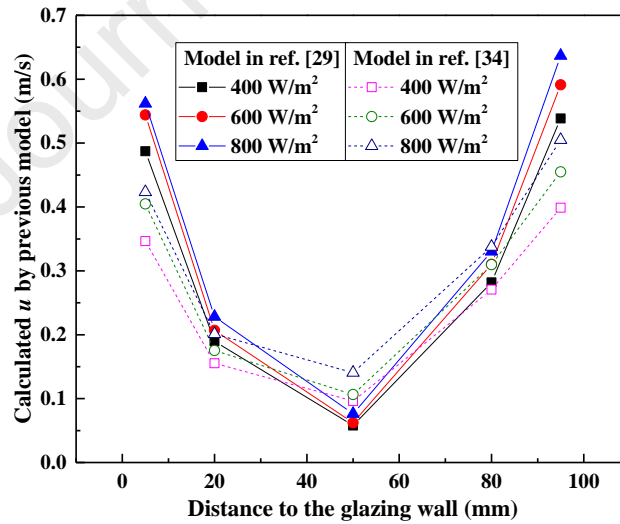


Fig. 5 Predicted airflow velocity in the cavity depth direction using the previous model, $h = 150\text{mm}$.

Figure 5 shows the predicted airflow velocity inside the solar chimney cavity by Eq. (3) based on the measured temperature, with a cavity height of 150 mm and no blockage. Higher predictions near sidewalls were obtained using the equation proposed by Hou *et al.* A slightly higher velocity was given at the centre position using the equation established by Eckert. However, compared with the experimental airflow velocity at the chimney cavity outlet, the current equation based on thermal boundary theory seriously overestimated the airflow velocity. Under these circumstances, the existing model is inapplicable. Therefore, an improved theoretical model must be developed to predict the practical airflow velocity in the solar chimney at the top of a tunnel.

3.2 Effect of blockage ratio on the airflow velocity

The blockage was located at the tunnel floor, where β was used to represent the blockage ratio $A_{blo.} / A_t$. The influence of blockage on airflow velocity at the solar chimney outlet is shown in Figs. 6 and 7. The airflow velocity was enhanced significantly under greater solar irradiation intensity. This is consistent with previous studies [35, 36]. Additionally, with the increase in cavity height, the airflow velocity improved for all blockage ratio conditions. The absorber area is increased with a larger cavity height, which means the total solar energy is absorbed to heat the fresh air inside the solar chimney. Thus, a larger air temperature gradient between the inlet and the outlet is gained to drive the airflow.

Generally, the airflow velocity close to the absorber was higher than that near the glazing wall. The maximum difference in the airflow velocity between the absorber and glazing exceeded 0.058 m/s under solar radiation of 400 W/m² with a cavity height of 300 mm. The average value of improvement airflow velocity close to the absorber than that near the glazing was 0.035, 0.033, and 0.04 m/s for cavity heights of 150, 250, and 300 mm, respectively. It can be seen that the cavity height has a limited impact on the velocity gradient between the glazing wall and the absorption wall.

From Figs. 6 and 7, the effect of the blockage ratio on airflow velocity at the outlet is insignificant for all solar intensities and cavity heights. This means that vehicles with relatively small cross-section areas, such as cars, in the urban tunnel have a limited impact on the solar chimney design. However, the effect of blockage on ventilation performance could not be neglected for a greater blockage ratio, such as in small cross-section urban tunnels or vehicles with relatively large cross-section areas. For instance, the bus, truck, or even metro train in the interstation tunnel would block the inlet of the solar chimney, and the influence on the ventilation performance of the solar chimney may be considerable. Under these circumstances, the effect of the blockage ratio on the ventilation performance of solar chimneys should be considered. However, the previous study and theoretical model have not considered the effect of vehicle blockage on solar performance. Therefore, a theoretical model to address the effect of the blockage ratio on the airflow velocity at the outlet is established in this work. This shows the quantitative relationship between ventilation performance and impact factors. Moreover, it benefits practical usage and engineering design by reducing the time cost.

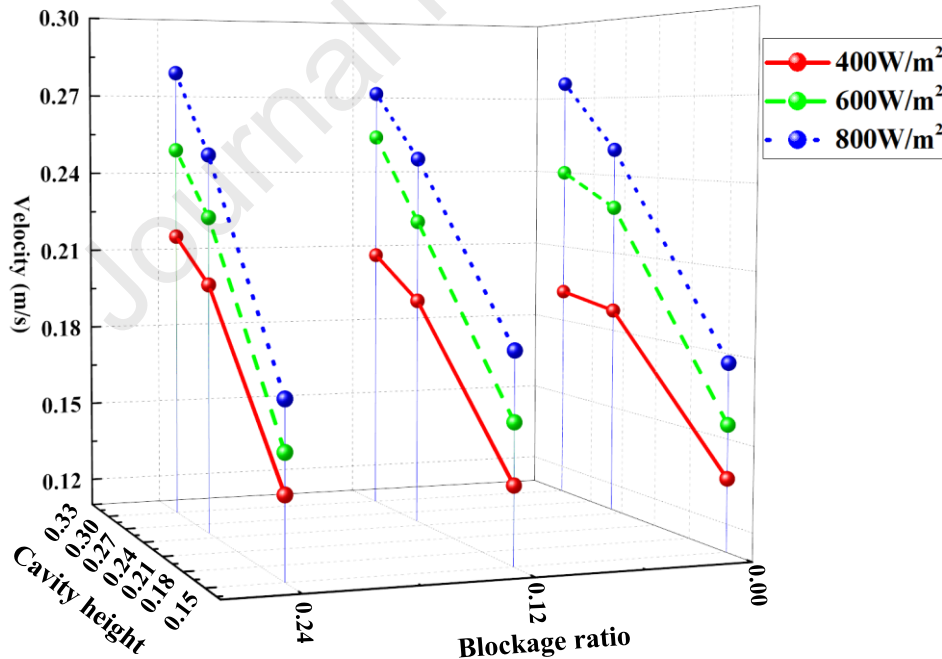


Fig. 6 Airflow velocity close to the glazing wall under different conditions.

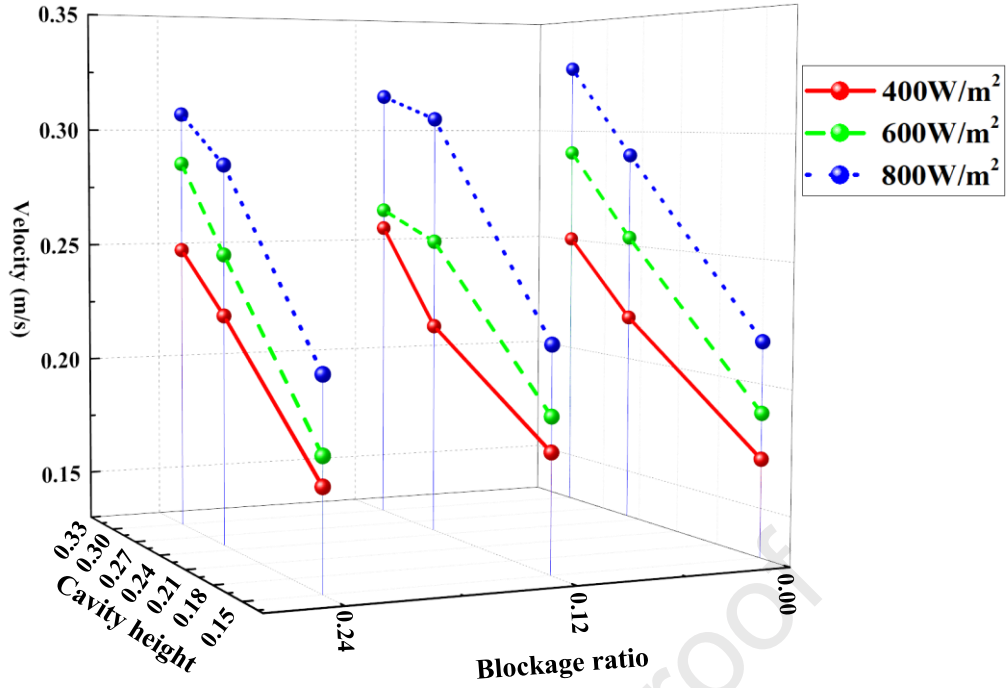


Fig. 7 Airflow velocity closed to absorber under different conditions.

4 Theoretical model

4.1 Analytical model for horizontal temperature

The temperature gradient is crucial for air inflow velocity inside the solar chimney cavity. The temperature close to the absorber wall is maximum due to absorbing the solar energy. Otherwise, the surface temperature of the glazing wall is relatively high. Figure 8 shows the temperature distribution along the cavity depth direction [10, 36], defined as horizontally two piecewise semi-parabolic temperature distributions. That means the temperature close to the glazing surface and the absorption wall archives peak value. In the cavity depth direction, the horizontal temperature from the opposite wall to the inside center decreases in a semi-parabolic form but with different attenuation rates. Thus, the two horizontal semi-parabolic is used to describe the temperature distribution in the cavity depth direction.

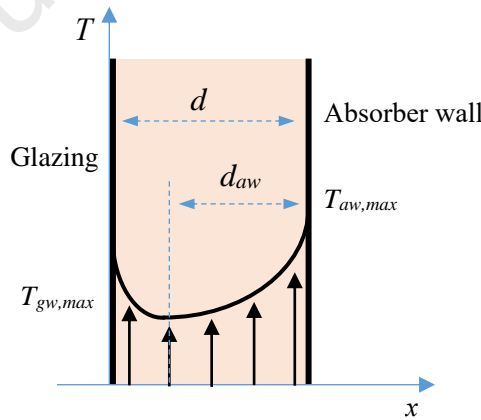


Fig. 8 Schematic of the temperature distribution in the cavity depth direction.

The absorption wall absorbs solar radiation to heat air, and some part of solar energy is absorbed by the glazing walls. As the conductive heat transfers, the temperature decreases from the sidewalls to the centre of the chimney cavity. The temperature attenuation of the two parts from the glazing and absorber walls can be considered a horizontal semi-parabolic distribution, respectively. Thus, the horizontal temperature from the opposite sidewall to the position of the lowest value is given by,

$$T = \frac{T_{max} - T_0}{d^{3/2}} x^{3/2} + T_0 \quad (6)$$

Based on the energy conservation equation, the absorbed energy can be given as

$$E_{aw} = \int_0^{d_{aw}} \kappa \left(\frac{T_{aw,max} - T_0}{d^{3/2}} x^{3/2} \right)^{3/2} dx \quad (7)$$

Therefore, the temperature rise close to the absorption wall is given by

$$\Delta T_{aw,max} = \left(\frac{E_{aw}}{\kappa} \frac{13}{4} \right)^{2/3} \frac{d^{3/2}}{d_{aw}^{13/6}} \quad (8)$$

Similarly, the temperature rises close to the glazing wall is obtained as

$$\Delta T_{gw,max} = \left(\frac{13}{4} \frac{E_{gw}}{\kappa} \right)^{2/3} \frac{d^{3/2}}{(d - d_{aw})^{13/6}} \quad (9)$$

At position d_{aw} , the temperature difference ΔT_{aw} equals ΔT_{gw} . Based on this boundary condition, the following equation can be obtained for d_{aw} ,

$$d_{aw} = \frac{\left(\frac{\tau}{1-\tau} \right)^{4/9} d}{1 + \left(\frac{\tau}{1-\tau} \right)^{4/9}} \quad (10)$$

The detailed derivation of the formula for horizontal temperature distribution can be found in Appendix A.

After substituting Eq. (10) into Eq. (8) and Eq. (9), the peak value of temperature rise is obtained. Then, the temperature rise can be calculated by substituting the maximum temperature rise into Eq. (6). The prediction of temperature by the proposed model under different solar radiation intensities is shown in Fig. 9, and compared the analytical value with experimental results. The temperature rise increases with $2/3$ power of solar radiation ($E^{2/3}$), that means the stronger radiation intensity achieves larger temperature gradient between cavity inlet and outlet. There is a good agreement between the predictions and experimental results, with an average error of less than 8%.

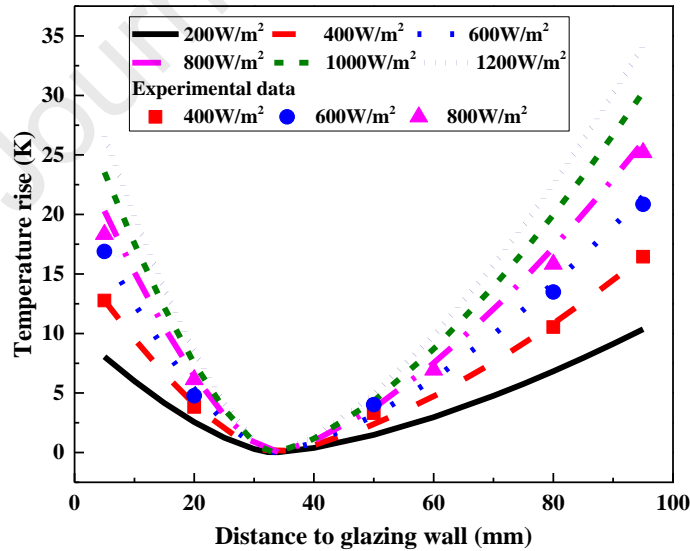


Fig.9 Profile of temperature rises in the cavity depth direction under different solar intensities.

4.2 Analytical model for airflow velocity

The volume flow rate at the outlet is a key parameter for estimating the performance of the solar chimney. However, from the experimental results and temperature profile, the airflow velocity along the cavity depth direction at the outlet should be first gained to integral the volume flow rate.

From the schematic of airflow in the tunnel and solar chimney in Fig. 1, the airflow will overcome the local resistance, friction resistance, and dynamic pressure at the outlet. The driving force of airflow comes from the density difference induced

by the air temperature gradient as absorbed solar radiation. The local resistance of airflow in the tunnel and chimney cavity are identified: entrance to the tunnel from outside, sudden contraction as blockage, entrance from the tunnel to the chimney channel (90° corner combined sudden contraction), and discharge outlet. There also exist friction resistances both in the tunnel and chimney cavity.

Based on the pressure analysis, the airflow velocity at the outlet is given as

$$u_{out} = A^* \sqrt{\frac{(\rho_0 - \rho_{out})gh}{\rho_{out}}} \quad (11)$$

$$A^* = \frac{4A_t^2 A_{blo.}^2}{\frac{\rho_{out}}{\rho_0} A_{out}^2 (A_{blo.}^2 \xi_{en} + \frac{A_{blo.}^2 \lambda L_t}{D_t} + A_t^2 \xi_{blo.}) + \frac{4A_t^2 A_{blo.}^2}{\rho_0} (\xi_{in} \rho_{out} + \frac{2\lambda h_c \rho_0 \rho_{out}}{(\rho_0 + \rho_{out}) D_c} + \rho_0 \xi_{out})} \quad (12)$$

Based on the ideal gas law, the relationship between air density and temperature can be given with less than 0.02% error [10],

$$\rho_0 T_0 = \rho_{out} T_{out} \quad (13)$$

Therefore, the airflow velocity at the outlet can be given as

$$u_{out} = A^* \sqrt{\frac{(T_{out} - T_0)gh}{T_0}} \quad (14)$$

The detailed derivation of the formula for airflow velocity at the outlet can be found in Appendix B.

The temperature profile at the outlet can be predicted by Eq. (6); substituting this temperature with Eq. (14) can predict the airflow velocity at the outlet.

Fig.10 Compares the airflow velocity calculated by Eq. (14) with the experimental results under different conditions. The predictions agree well with the experimental data for all blockage ratios. The average errors between the analytical model and experimental velocity are 3.5%, 3.6%, and 2.2% under the blockage ratio of 0, 0.12, 0.24, respectively.

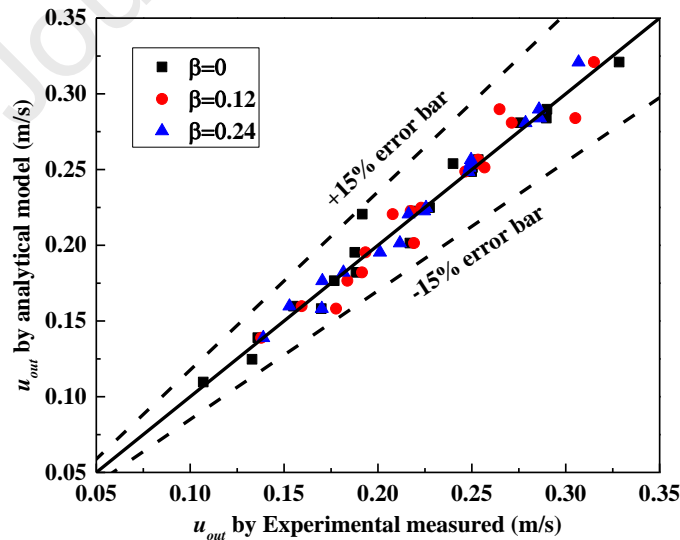


Fig.10 Comparisons of airflow velocity at the outlet between experiments and predictions.

4.3 Volume flow rate at the outlet

The volume flow rate is an important parameter to estimate the ventilation performance of a solar chimney configuration, which is a standard parameter for evaluating indoor air quality. Therefore, the volume flow rate through the solar chimney should be finalized. The ventilation rate through a sharp orifice can be given by

$$V = C_d A u \quad (15)$$

From Eq. (14), the airflow velocity at the outlet varies with the outlet temperature. Thus, the velocity integral in the cavity depth direction is used to evaluate the volume flow rate through the outlet,

$$V_{out} = C_d w \int_0^{d-d_{aw}} A^* \sqrt{\frac{(T_{aw,max} - T_o) g h x^{3/2}}{d^{3/2} T_o}} dx + \int_0^{d-d_{aw}} A^* \sqrt{\frac{(T_{gw,max} - T_o) g h x^{3/2}}{d^{3/2} T_o}} dx \quad (16)$$

After integrating Eq. (16), the volume flow rate can be given by,

$$V_{out} = C_d w A^* \frac{4}{7} \sqrt{\frac{g h}{d^{3/2} T_o}} \frac{d^{7/4}}{d^{3/2} T_o} \Delta T_{aw,max}^{1/2} + \Delta T_{gw,max}^{1/2} (d - d_{aw})^{7/4} \quad (17)$$

Fig. 11 quantifies the volume flow rate under different conditions. The analytical model suggests the volume flow rate V_{out} varied with $E^{1/3}$, which is less than the power of $E^{0.5-0.572}$ applied in buildings [38]. However, this is consistent with the previous power of $E^{0.34}$ for a tunnel considering horizontal parabolic temperature decay [10]. The volume flow rate linearly increased with $h^{0.67}$; this power of cavity height is close to the previous result of $h^{0.69}$ in tunnels, but larger than the previous study about building solar chimney $V_{out} \propto h^{1/2-2/3}$ [38]. A slight decline of V_{out} occurs with the larger blockage ratio. Thus, the effect of vehicle blockage on the ventilation rate is limited under $\beta < 0.6$.

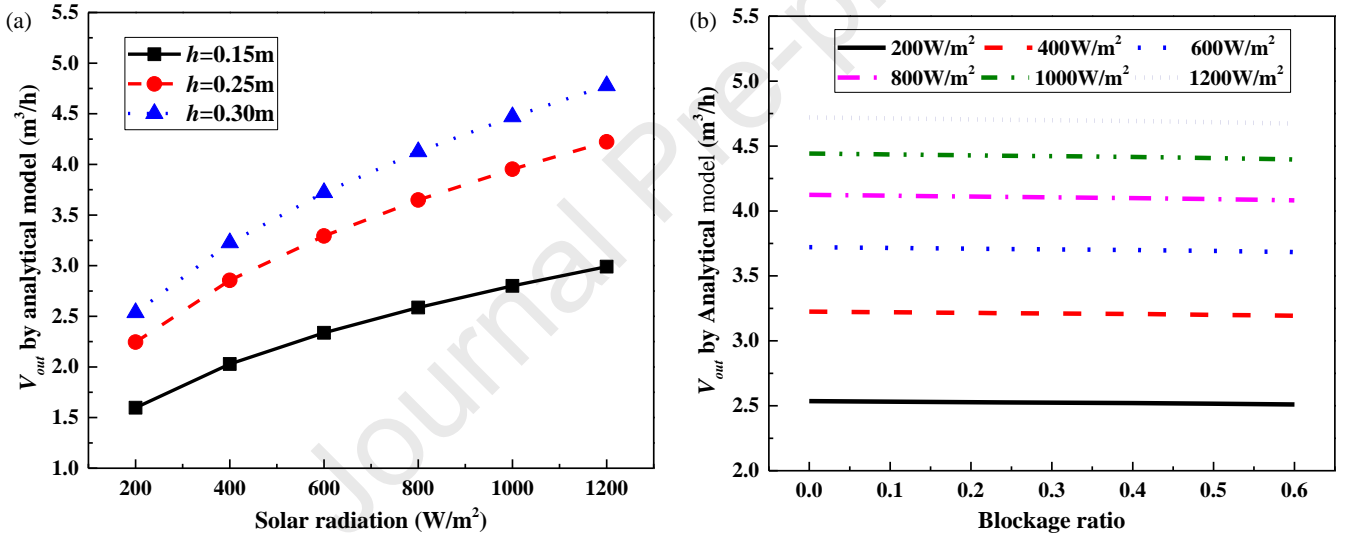


Fig.11 Volume flow rate by an analytical model, (a) varied solar intensities $\beta=0$, (b) varied β , $h=0.3m$.

Full-scale results are urgently needed to validate the accuracy of the analytical model. However, the experimental ventilation rate at the outlet for the solar chimney adopted in the tunnel is not found in the literature. Therefore, the experimental small-scale tunnel was transformed into a full-scale one and a numerical code fire dynamic simulator (FDS) was used to simulate the airflow. Validation of FDS was conducted in a previous study [7, 10, 24].

Fig.12 Shows the volume flow rate in a full-scale tunnel, comparing the analytical model and numerical results. The comparison is made at a fixed cavity height ($h=5m$), blockage ratio ($\beta=0$) and solar intensity ($800W/m^2$). The analytical model over a cavity height of 5 m without blockage shows over-predictions by 4-11% overall solar radiation. The friction resistance coefficients fixed at 0.02 in the analytical model may differ from the numerical values due to the surface roughness. Additionally, some heat losses from two sidewalls are not covered by thermal insulation materials in numerical simulations. Despite the vehicle blockage, the 6.3% average error between the analytical model and numerical code indicates an acceptable error caused by surface roughness and heat loss. The analytical model suggests that the ventilation rate $V_{out} \propto e^{5.3\beta}$. The average error is 2.5% over the blockage ratios, with the analytical model over-predicting. This is in reasonable accuracy as the limited effect of blockage on the ventilation rate.

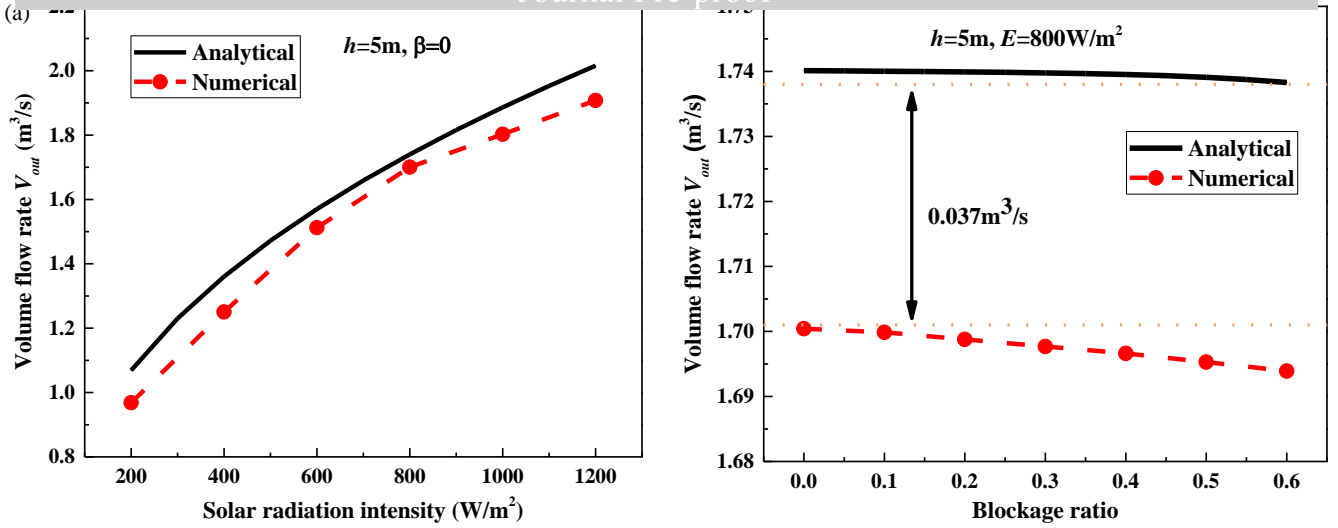


Fig.12 A comparison of the ventilation rate predicted by analytical model and simulations: (a) solar intensity and (b) blockage ratio.

Additionally, the numerical results of the ventilation rate for a case tunnel in Chongqing, China (with a dimension of 815 m length, 9.25 m width and 5m height) are compared with the calculated value by Eq. (17). The solar chimney was installed at the top of the tunnel center. The solar radiation is fixed at 800W/m^2 . The cavity depth is 2m, the cavity width varies from 3 m to 9 m under a certain cavity height of 5m, and the cavity height ranges from 1 m to 5 m for a given cavity width of 3 m. Fig. 13 shows the comparison of ventilation rate between numerical data and calculated value.

From Fig.13 (a) The ventilation rate shows a linear rise with cavity width. Under this circumstance, the air change rate and air quality inside the tunnel can be improved under a wider cavity. Thus, to achieve ventilation performance, the top solar chimney can be designed as wide as possible for the practical tunnel. From Fig.13 (b) The ventilation rate was significantly accelerated under higher cavities, but the growth rate weakened when the cavity height increased gradually. Thus, the cavity height should be relatively high but not too high. Because too height of the cavity is unable to significantly improve the ventilation rate but rising construction costs and difficulty. Under the solar chimney integrated into this tunnel case, the average errors of ventilation rate throughout the solar chimney between predictions and numerical results are 6.3% and 6% for different cavity widths and heights, respectively. Overall, the predicted value by Eq. (17) is in good agreement with the numerical results. The solar chimney with a 9 m width and 5 m height can gain the optimal ventilation rate for this tunnel.

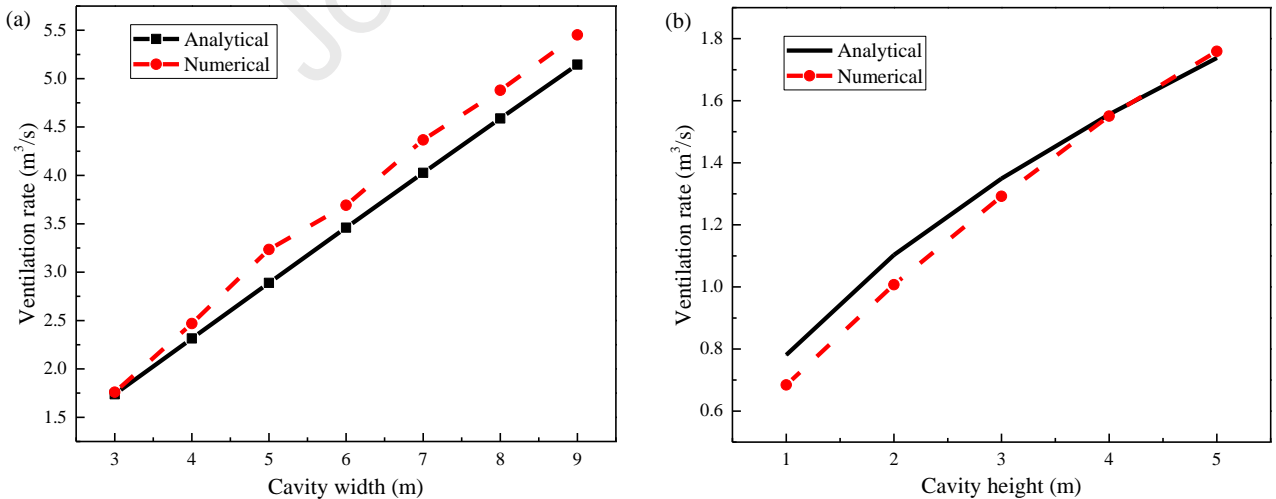


Fig.13 A comparison of the ventilation rate for a case tunnel:(a) different cavity widths and (b) different cavity heights.

5 Conclusions

This study conducted a comprehensive series of experiments to thoroughly investigate the ventilation performance of a solar chimney integrated into a tunnel. By considering the horizontally two-piecewise semi-parabolic temperature distribution, theoretical models were developed to accurately predict the outlet temperature, outflow velocity, and volume flow rate

throughout the solar chimney, while also accounting for the impact of vehicle blockage. The main conclusions drawn from this research can be summarized as follows:

(1) The temperature at the outlet exhibits a direct correlation with increased solar radiation and greater cavity height, with the temperature variation showing a positive relationship with $E^{2/3}$. Additionally, the temperature near the absorption wall is higher than that near the glazing surface. Along the cavity depth direction, the temperature undergoes attenuation following two-piecewise semi-parabolic curves from the glazing wall and absorption wall to the position of the lowest temperature. A theoretical model has been successfully established to predict the temperature rise at the outlet, demonstrating excellent agreement with the experimental results.

(2) The airflow velocity near the absorption wall surpasses that near the glazing wall. The positive effects of cavity height and solar radiation on the airflow velocity at the outlet are significant, while the blockage ratio exhibits only a limited influence on the airflow velocity. A robust theoretical model for the outflow velocity has been developed, accounting for the effects of vehicle blockage, with an average error of less than 3.6%.

(3) The ventilation rate at the outlet can be accelerated by wider and higher cavities, as more solar radiation is absorbed. A comprehensive mathematical model for the volume flow rate of the solar chimney in a tunnel has been formulated, revealing a linear increase in the volume flow rate with $E^{1/3}$. This model effectively addresses the influence of solar chimney configuration on the ventilation rate. Numerical simulations have successfully validated the theoretical evidence presented.

In summary, this study significantly contributes to the understanding of solar chimney performance in tunnel ventilation systems. The established theoretical models for outlet temperature, outflow velocity, and volume flow rate offer practical and accurate design tools. These findings have substantial implications for architects and engineers seeking to optimize solar chimney configurations, ultimately promoting the implementation of energy-efficient and sustainable solutions in urban tunnel designs.

CRedit authorship contribution statement

Youbo Huang: Formal analysis, Project administration, supervision, writing the original draft. **Xi Liu:** Data curation, writing, review & editing. **Long Shi:** Conceptualization, Writing - review & editing, Methodology, Supervision, Resources. **Bingyan Dong:** Data curation, writing, review & editing. **Hua Zhong:** Methodology, Writing - review & editing.

Declaration of Competing Interest

The authors declare that they have no known competing financial interests or personal relationships that could have appeared to influence the work reported in this paper.

Acknowledgements

The authors acknowledge support from the Research Foundation of Chongqing for graduated doctor [Grant No. CSTB2022BSXM-JCX0151], the National Natural Science Foundation of China (NSFC) [Grant No. 52104185, 52274235], the Natural Science Foundation of Chongqing, China [Grant No. cstc2021jcyj-msxmX0919], the Fundamental Research Funds for the Central Universities [Grant No. WK2320000056], the Natural Science Foundation of Sichuan Province [Grant No. 2022NSFSC0278], the Science and Technology Research Program of Chongqing Municipal Education Commission [Grant No. KJQN202101527].

Appendix A. Horizontal temperature calculation

The absorption wall absorbed solar radiation to heat air, and the air temperature decreased gradually away from the absorber due to conductive heat transfer. Some parts of solar energy have been absorbed by glazing walls. The energy conservation equation in the chimney cavity can be given by

$$E = \rho_c c_p V_{out} (T_c - T_0) \quad (A1)$$

The total energy absorbed by the absorption wall is

$$E_{aw} = \tau w h q_{sol} \quad (A2)$$

The solar energy absorbed by the glazing wall is

$$E_{gw} = \varepsilon w h q_{sol} \quad (A3)$$

where τ is the transmissivity of the glazing wall, and ε is the absorptivity of the glazing wall.

Based on the energy conservation equation, the energy within minuteness Δx can be given by

$$\Delta E = \rho_c c_p \Delta V_{out} (T - T_0) \quad (A4)$$

where ΔV_{out} is the volume flow rate at the outlet within Δx ,

$$\Delta V_{out} = C_d w \Delta x \sqrt{\frac{2(T - T_0)gh}{T_0}} \quad (A5)$$

Combined Eqs. (A4) and Eq. (A5), the following equation can be gained:

$$\Delta E = \kappa (T_c - T_0)^{3/2} \Delta x, \quad \kappa = \rho_c c_p C_d w \sqrt{\frac{2gh}{T_0}} \quad (A6)$$

where κ is the coefficient.

The temperature decreased from the sidewall to the centre of the chimney cavity. The temperature attenuation of the two parts from the glazing and absorber walls can be considered a horizontal semi-parabolic distribution, respectively. Thus, the horizontal temperature from the opposite sidewall to the position of the lowest value is given by,

$$T = \frac{T_{max} - T_0}{d^{3/2}} x^{3/2} + T_0 \quad (A7)$$

where d is the cavity depth in m and x is the distance away from the side wall.

Substituted Eq. (A7) into Eq. (A6), the absorbed energy can be given as

$$E_{aw} = \int_0^{d_{aw}} \kappa \left(\frac{T_{aw,max} - T_0}{d^{3/2}} x^{3/2} \right)^{3/2} dx \quad (A8)$$

where d_{aw} is the horizontal distance from the absorber wall to the position of lowest temperature in m.

After integrating Eq. (A8), the following equation is given by

$$E_{aw} = \kappa \left(\frac{T_{aw,max} - T_0}{d^{3/2}} \right)^{3/2} \frac{4}{13} d_{aw}^{13/4} \quad (A9)$$

Thus, the temperature rises close to the absorption wall given by

$$\Delta T_{aw,max} = \left(\frac{E_{aw}}{\kappa} \frac{13}{4} \right)^{2/3} \frac{d^{3/2}}{d_{aw}^{13/6}} \quad (A10)$$

where $T_{aw,max}$ and $T_{gw,max}$ are the temperatures close to the absorption and glazing walls in K.

Similarly, the temperature rises close to the glazing wall is obtained as

$$\Delta T_{gw,max} = \left(\frac{13 E_{gw}}{4 \kappa} \right)^{2/3} \frac{d^{3/2}}{(d - d_{aw})^{13/6}} \quad (A11)$$

At position d_{aw} , the temperature difference ΔT_{aw} equals ΔT_{gw} . Based on this boundary condition, the following equation can be obtained,

$$\frac{\left(\frac{E_{aw}}{\kappa} \frac{13 d^{9/4}}{4 d_{aw}^{13/4}} \right)^{3/2}}{d^{3/2}} d_{aw}^{3/2} = \frac{\left(\frac{E_{gw}}{\kappa} \frac{13 d^{9/4}}{4 (d - d_{aw})^{13/4}} \right)^{3/2}}{d^{3/2}} (d - d_{aw})^{3/2} \quad (A12)$$

Substituted Eqs. (A2) and (A3) into Eq. (A12), it is given by

$$\frac{\left(\frac{\tau whq_{sol}}{\kappa} \frac{13 d^{9/4}}{4 d_{aw}^{13/4}} \right)^{3/2}}{d^{3/2}} d_{aw}^{3/2} = \frac{\left(\frac{(1-\tau) whq_{sol}}{\kappa} \frac{13 d^{9/4}}{4 (d - d_{aw})^{13/4}} \right)^{3/2}}{d^{3/2}} (d - d_{aw})^{3/2} \quad (A13)$$

Thus, the distance of d_{aw} is given by

$$d_{aw} = \frac{\left(\frac{\tau}{1-\tau} \right)^{4/9} d}{1 + \left(\frac{\tau}{1-\tau} \right)^{4/9}} \quad (A14)$$

Appendix B. Horizontal velocity calculation

The local resistance can be calculated using the,

$$\Delta P_{\xi_j} = \frac{1}{2} \xi_j \rho u^2 \quad (B1)$$

The local resistance coefficients ξ at the entrance and outlet are 0.5 and 1.0, respectively [37]. The local resistance coefficient of sudden contraction is related to the blockage ratio, where $\xi_{blo.} = 0.5\beta$. The resistance coefficient from the tunnel to the chimney includes the sudden contraction and right-angle turn.

The local resistance can be given by,

$$\Delta P_{\xi} = \frac{1}{2} \xi_{en} \rho_0 u_t^2 + \frac{1}{2} \xi_{blo.} \rho_0 u_t^2 + \frac{1}{2} \xi_{in} \rho_0 u_{blo.}^2 + \frac{1}{2} \xi_{out} \rho_c u_{out}^2 \quad (B2)$$

where ΔP_{ξ} is the local resistance in Pa. As the temperature difference along the tunnel is minimal, the temperature and density are almost the same. The ρ_c is the air density before the outlet, almost close to the density at the outlet. Thus, the density at outlet ρ_{out} is used to replace the ρ_c during calculating the local resistance.

The blockage of 0.5 m length is located at the chimney channel inlet, and the blockage length is small enough to neglect during calculating the friction resistance in this study. The friction resistance can be given by,

$$\Delta P_{\lambda} = \frac{1}{2} \frac{L_t}{D_t} \rho_0 u_t^2 + \frac{1}{2} \frac{h}{D_c} \rho_c u_c^2 \quad (B3)$$

where ΔP_{λ} is the friction resistance in Pa, D_t and D_c are the hydraulic diameters for the rectangular and chimney channels.

The absorbed solar energy heats the air, meanwhile, the stack effect occurs due to the density gradient. The pressure difference drives the airflow from the tunnel entrance to the chimney channel which depends on the density and height difference. Based on the pressure difference, the following equation can be given as

$$\Delta P_{\xi} + \Delta P_{\lambda} = (\rho_0 - \rho_c) gh \quad (B4)$$

Under steady conditions, the mass flow inside the tunnel and chimney channel remains stable. Based on this, the mass conversation equation can be given as Eq. (B5). Notes that assumed the intake air from both ends of the tunnel are the same.

$$2\rho_0 A_t u_t = 2\rho_0 A_{blo.} u_{blo.} = \rho_0 A_{in} u_{in} = \rho_{out} A_{out} u_{out} = \rho_c A_c u_c \quad (B5)$$

The cross-sectional area at the inlet, outlet, and the inside channel is the same, $A_{in} = A_{out} = A_c$. The blockage region's area equals tunnel area minus blockage cross-section area, $A_{blo.} = (1-\beta) A_t$.

The air density inside the chimney cavity decreased linearly from the inlet to the outlet as the linear temperature distribution [10]. Thus, the static pressure can be given by Eq. (B6). The air density inside the channel can be used as the average value, $\rho_c = 1/2(\rho_0 + \rho_{out})$.

$$\rho_c g h = \int_0^h \rho g dH = \frac{1}{2}(\rho_0 + \rho_{out}) g h \quad (B6)$$

Substituting Eqs. (B2) and (B3) into Eq. (B4), all the airflow velocity transferred to u_{out} based on Eq. (B5), and it is obtained,

$$\begin{aligned} & \xi_{en} \rho_0 \frac{\rho_{out} A_{out} u_{out}}{2\rho_0 A_t} \frac{\ddot{\theta}^2}{\theta} + \frac{L_t}{D_t} \rho_0 \frac{\rho_{out} A_{out} u_{out}}{2\rho_0 A_t} \frac{\ddot{\theta}^2}{\theta} + \xi_{blo.} \rho_0 \frac{\rho_{out} A_{out} u_{out}}{2\rho_0 A_{blo.}} \frac{\ddot{\theta}^2}{\theta} + \xi_{in} \rho_0 \frac{\rho_{out} u_{out}}{\rho_o} \frac{\ddot{\theta}^2}{\theta} \\ & + \frac{h}{D_c} \frac{1}{2} (\rho_0 + \rho_{out}) \frac{\rho_{out} u_{out}}{\frac{1}{2}(\rho_0 + \rho_{out})} \frac{\ddot{\theta}^2}{\theta} + \xi_{out} \rho_{out} u_{out}^2 = (\rho_0 - \rho_{out}) g h \end{aligned} \quad (B7)$$

Simplified the equation (B7), it is given the airflow velocity at the outlet as

$$u_{out} = A^* \sqrt{\frac{(\rho_0 - \rho_{out}) g h}{\rho_{out}}} \quad (B8)$$

$$A^* = \frac{4A_t^2 A_{blo.}^2}{\frac{\rho_{out}}{\rho_0} A_{out}^2 (A_{blo.}^2 \xi_{en} + \frac{A_{blo.}^2 \lambda L_t}{D_t} + A_t^2 \xi_{blo.}) + \frac{4A_t^2 A_{blo.}^2}{\rho_0} (\xi_{in} \rho_{out} + \frac{2\lambda h_c \rho_0 \rho_{out}}{(\rho_0 + \rho_{out}) D_c} + \rho_0 \xi_{out})} \frac{\ddot{\theta}^2}{\theta} \quad (28)$$

Based on the ideal gas law, the relationship between air density and temperature can be given with less than 0.02% error [10],

$$\rho_0 T_0 = \rho_{out} T_{out} \quad (B9)$$

Based on Eq. (B9), the airflow velocity at the outlet can be given by,

$$u_{out} = A^* \sqrt{\frac{(T_{out} - T_o) g h}{T_o}} \quad (B10)$$

The temperature profile at the outlet can be predicted by Eq. (A7); substituting this temperature with Eq. (B10) can predict the airflow velocity at the outlet.

References

- [1] F. Jiao, Z. Du, Y. D. Wong, S. He, F. Xu, and H. Zheng, Self-explaining performance of visual guiding facilities in urban road tunnels based on speed perception, *Tunn. Undergr. Sp. Technol.*, 2022, 122, 104371.
- [2] L. Xu *et al.*, Spatial-temporal prediction of the environmental conditions inside an urban road tunnel during an incident scenario, *Build. Environ.*, 2022, 212, 108808.
- [3] H. Wang, Z. Jiang, G. Zhang, F. Zeng, Parameter analysis of jet tunnel ventilation for long distance construction tunnels at high altitude, *J. Wind Eng. Ind. Aerodyn.*, 2022, 228, 105128.
- [4] Y. Hong, C. Fu, B. Merci, Numerical analysis of the performance of a PID control based real-time mechanical ventilation system to prevent smoke back-layering in tunnel fires, *Tunn. Undergr. Sp. Technol.*, 2022, 128, 104639.
- [5] C. Guo, M. Wang, L. Yang, Z. Sun, Y. Zhang, J. Xu, A review of energy consumption and saving in extra-long tunnel operation ventilation in China, *Renew. Sustain. Energy Rev.*, 2016, 53, 1558–1569.
- [6] M. López González, M. Galdo Vega, J. M. Fernández Oro, E. Blanco Marigorta, Numerical modeling of the piston effect in longitudinal ventilation systems for subway tunnels, *Tunn. Undergr. Sp. Technol.*, 2014, 40, 22–37.
- [7] L. Shi, A. Ziem, G. Zhang, J. Li, S. Setunge, Solar chimney for a real building considering both energy-saving and fire safety – a case study, *Energy Build.*, 2020, 221, 110016.
- [8] Z. Zhang, H. Zhang, Y. Tan, H. Yang, Natural wind utilization in the vertical shaft of a super-long highway tunnel and its energy saving effect,” *Build. Environ.*, 2018, 145, 140–152.
- [9] C. H. Yoon, M. S. Kim, J. Kim, The evaluation of natural ventilation pressure in Korean long road tunnels with vertical shafts, *Tunn. Undergr. Sp. Technol.*, 2006, 21, 3–4.
- [10] X. Cheng, Z. C. Shi, K. Nguyen, L. H. Zhang, Y. Zhou, G. M. Zhang, J. H. Wang, L. Shi, Solar chimney in tunnel considering energy-saving and fire safety, *Energy*, 2020, 210, 118601.
- [11] H. H. Al-Kayiem, K. V. Sreejaya, A. O. Chikere, Experimental and numerical analysis of the influence of inlet configuration on the performance of a roof top solar chimney, *Energy Build.*, 2018, 159, 89–98, 2018.
- [12] R. Vargas-López *et al.*, Mathematical models of solar chimneys with a phase change material for ventilation of buildings: A review using global energy balance, *Energy*, 2019, 170, 683–708.
- [13] M. K. Hasan, A. Gross, L. Bahrainirad, H. F. Fasel, Investigation of collector flow for 1:30 scale solar chimney power plant model, *Sol. Energy*, 2022, 241, 220–230.
- [14] F. Murena, I. Gaggiano, B. Mele, Fluid dynamic performances of a solar chimney plant: Analysis of experimental data and CFD modelling, *Energy*, 2022, 249, 123702.
- [15] S. H. Fallah, M. S. Valipour, Numerical investigation of a small scale sloped solar chimney power plant, *Renew. Energy*, 2022, 183, 1–11.
- [16] H. Zhang *et al.*, A critical review of combined natural ventilation techniques in sustainable buildings, *Renew. Sustain. Energy Rev.*, 2020, 141, 110795.
- [17] T. Miyazaki, A. Akisawa, T. Kashiwagi, The effects of solar chimneys on thermal load mitigation of office buildings under the Japanese climate, *Renew. Energy*, 2006, 31, 987–1010.
- [18] H. M. Maghrabie *et al.*, A review of solar chimney for natural ventilation of residential and non-residential buildings, *Sustain. Energy Technol. Assessments*, 2022, 52, 102082.
- [19] R. Tariq *et al.*, Digital twin models for optimization and global projection of building-integrated solar chimney, *Build. Environ.*, 2022, 213, 108807.
- [20] B. Zamora, Determining correlations for solar chimneys in buildings with wind interference: A numerical approach, *Sustain. Energy Technol. Assessments*, 2021, 48, 101662.
- [21] Y. Yao, K. He, M. Peng, L. Shi, X. Cheng, H. Zhang, Maximum gas temperature rise beneath the ceiling in a portals-sealed tunnel fire, *Tunn. Undergr. Sp. Technol.*, 2018, 80, 10–15, 2018.
- [22] Y. Huang *et al.*, Experimental investigation on maximum gas temperature beneath the ceiling in a branched tunnel fire, *Int. J. Therm. Sci.*, 2019, 145, 105997.
- [23] X. Jiang, Y. Xiang, Z. Wang, Y. Mao, H. Park, A numerical study on the effect of the shaft group arrangement on the natural ventilation performance in tunnel fires, *Tunn. Undergr. Sp. Technol.*, 2020, 103, 103464.

- [24] H. Zhang, T. Tao, G. Zhang, J. Li, S. Setunge, L. Shi, Impacts of storey number of buildings on solar chimney performance: A theoretical and numerical approach, *Energy*, 2022, 261, 125200.
- [25] K. T. Andersen, Theory for natural ventilation by thermal buoyancy in one zone with uniform temperature, *Build. Environ.*, 2003, 38, 1281–1289.
- [26] A. Sengupta, D. P. Mishra, S. K. Sarangi, Computational performance analysis of a solar chimney using surface modifications of the absorber plate, *Renew. Energy*, 2022, 185, 1095–1109.
- [27] G. Q. He, D. Lv, Distributed heat absorption in a solar chimney to enhance ventilation, *Sol. Energy*, 2022, 238, 315–326.
- [28] J. Gong, K. Xian, H. Liu, L. Wai, P. Seng, A novel staggered split absorber design for enhanced solar chimney performance, *Build. Environ.*, 2022, 224, 109569.
- [29] Y. C. Hou, H. Li, A. G. Li, Experimental and theoretical study of solar chimneys in buildings with uniform wall heat flux, *Sol. Energy*, 2019, 193, 244–252.
- [30] X. Cheng, L. Shi, P. Dai, G. Zhang, H. Yang, J. Li, Study on optimizing design of solar chimney for natural ventilation and smoke exhaustion, *Energy Build.*, 2018, 170, 145–156.
- [31] S. Suhendri, M. Hu, Y. Su, J. Darkwa, S. Riffat, Parametric study of a novel combination of solar chimney and radiative cooling cavity for natural ventilation enhancement in residential buildings, *Build. Environ.*, 2022, 225, 109648.
- [32] Y. Tao, H. Zhang, D. Huang, C. Fan, J. Tu, L. Shi, Ventilation performance of a naturally ventilated double skin façade with low-e glazing, *Energy*, 2021, 229, 120706.
- [33] A. Salama, Velocity Profile Representation for Fully Developed Turbulent Flows in Pipes: A Modified Power Law, *Fluids*, 2021, 6, 100369.
- [34] Eckert, E.R., Jackson, T.W., 1950. Analysis of turbulent free-convection boundary layer on flat plate (No. NACA-TN-2207). National Aeronautics and Space Administration, Washington DC.
- [35] Y. Tao, X. Fang, M. Y. L. Chew, L. Zhang, J. Tu, L. Shi, Predicting airflow in naturally ventilated double-skin facades: theoretical analysis and modelling, *Renew. Energy*, 2021, 179, 1940–1954.
- [36] J. Kong, J. Niu, C. Lei, A CFD based approach for determining the optimum inclination angle of a roof-top solar chimney for building ventilation, *Sol. Energy*, 2020, 198, 555–569.
- [37] G. Q. He, Q. Wu, Z. G. Li, W. Q. Ge, D. Lv, L. Cong, Ventilation performance of solar chimney in a test house: Field measurement and validation of plume model, *Build. Environ.*, 2021, 193, 2021, 107648.
- [38] L. Shi, G. Zhang, W. Yang, D. Huang, X. Cheng, S. Setunge, Determining the influencing factors on the performance of solar chimney in buildings, *Renew. Sustain. Energy Rev.*, 2017, 88, 223–238.

- Enhancing tunnel ventilation: experimental investigation of solar chimney integration.
- Temperature distribution analysis: unveiling the intriguing two-piecewise semi-parabolic decay.
- Optimizing ventilation efficiency: negligible impact of vehicle blockage on solar chimney.
- Accurate design tools: theoretical models for temperature and ventilation prediction.

Declaration of interests

☒ The authors declare that they have no known competing financial interests or personal relationships that could have appeared to influence the work reported in this paper.

☐ The authors declare the following financial interests/personal relationships which may be considered as potential competing interests: